Bremsstrahlung Imaging Using the Gamma Camera: Factors Affecting Attenuation

Laurence P. Clarke, Shelby J. Cullom*, Robin Shaw, Curt Reece, Bill C. Penney, Michael A. King, and Martin Silbiger

Department of Radiology, College of Medicine, University of South Florida, Tampa, Florida, and Department of Nuclear Medicine, University of Massachusetts Medical Center, Worcester, Massachusetts

Quantitative imaging of bremsstrahlung from pure beta emitters is proposed as a means for in vivo management of antibody therapy. The method involves the use of high-energy collimation, an empirically selected broad photon energy window to enhance detector sensitivity, and a Wiener restoration filter to compensate for system blur. The measured and filtered data were obtained for an idealized scattering medium and isolated spherical sources. An effective linear attenuation coefficient of about 0.13 cm^{-1} was determined from the raw image data of ^{32}P. A coefficient of 0.14 cm^{-1} was determined after the images were restored using the Wiener filter. The measured attenuation was not significantly dependent on the size of the region of interest or the size of the source. Its variation was within the experimental error of measurement (±5%). The measured sensitivity (6×10^{-6} cps/Bq) was sufficient for imaging therapy doses of ^{32}P or ^{90}Y.

J Nucl Med 1992; 33:161-166

Quantitative imaging of bremsstrahlung, using a gamma camera, has been recently proposed as a basis for the in vivo management of antibody therapy using pure beta emitters such as ^{32}P (E_{max} = 1.71 MeV, $T_{½}$ = 14.3 days) or ^{90}Y (E_{max} = 2.27 MeV, $T_{½}$ = 2.7 days) (*1–3*). Electrons of such energies result in relatively low photon yield in tissues of small atomic number. Therefore, in bremsstrahlung imaging, a broad range of photon energies should be imaged in order to obtain the necessary detector sensitivity (*1–7*). In addition, many of the assumptions employed in single photon imaging should be reconsidered when imaging bremsstrahlung. The collimated system response, detector shielding, and photon transport must be considered as energy dependent processes (*1*). Attenuation correction methods must employ effective attenuation coefficients since the attenuation coefficient may not be constant over the range of photon energies imaged. Photons from the lower energy range have higher probability of undergoing scatter processes as predicted by transport models. Photons from the higher energy range have an increased probability of transversing the collimator septum and detector crystal. These processes result in significant image degradation (*4–7*). The cumulative effect can still be characterized with the system modulation transfer function (MTF) and should allow the implementation of restoration filters as reported for single photon emitters (*8–10*).

The measured attenuation for single photon emitters has been shown to be dependent on various factors including: (a) the type of the collimator which is related to the variation of the resolution response characteristics with distance, (b) the size of the selected energy window, (c) the size of the source, (d) the region of interest (ROI) used to obtain measured external counts (*11–16*), and (e) the resolution recovery filters (*8,10*). These factors are particularly important in the case of high photon energies, e.g., ^{131}I (364 keV), when conventional collimators are employed (*14*). We have previously investigated the use of a long-bore, high-energy collimator which results in less variation in resolution with distance (*3,13,16*). This collimator should approach the requirements for the application of stationary restoration filters in bremsstrahlung imaging (*13*).

The work reported here was directed at performing experimental measurements of an effective attenuation coefficient for bremsstrahlung using the above high energy collimator and a Wiener restoration filter (*10*). The dependence of the attenuation on ROI size, source size, and filter was also determined. Measurements were performed with the long-lived radionuclide ^{32}P. This can serve as a model for ^{90}Y or other beta-emitting radionuclides of interest which have a shorter half-life and comparable electron energy.

MATERIALS AND METHODS

Detector System and Collimation

The gamma camera employed was a Picker International Dyna Camera (Model 5/37) with a square (368 × 368 mm) NaI(Tl) crystal 9.5-mm thick. The detector side wall shielding was de-

Received Apr. 30, 1991; revision accepted Jul. 22, 1991.

For reprints contact: Laurence P. Clarke, PhD, Associate Professor of Radiology and Physics, Department of Radiology, MDC 17, College of Medicine, University of South Florida, 12901 North Bruce B Downs Blvd., Tampa, FL 33612.

* Current address: Dept. of Nuclear Medicine, Emory University School of Medicine, Atlanta, GA.

TABLE 1
Design Parameters of the Collimator

Square geometry (mm)	368 × 368
Bore length (mm)	70.6
Effective hole diameter (mm)	3.175
Septal thickness (mm)	1.143
Theoretical leakage (200–400 keV)	<1%

The effective hole diameter relates to a circle circumscribing the hexagon shaped apertures. The theoretical leakage is estimated using an optimal ray technique through the collimator septa.

signed for photon energies up to 511 keV. The collimator was designed with a bore length of 70.6 mm to reduce the variation in resolution with distance for medium to high single-photon energies. Other design parameters of the collimator are listed in Table 1 (*11–12*). Although the longer bore of the collimator results in a reduction of its geometrical efficiency, the sensitivity is still sufficient to measure therapy doses of radioactivity.

Table 2 summarizes the resolution parameters, full width at half maximum (FWHM) and full width at tenth maximum (FWTM) of the point spread function (PSF), obtained from various depths of the point source in the scattering medium (*1, 2,13*). At a source depth of 10 cm, i.e., a total distance of 15 cm from the collimator face, the measured values of the FWHM and FWTM for the single detector were 16.8 mm and 25.2 mm, respectively. The resolution obtained was comparable to that observed for single-photon imaging of ^{99m}Tc (140 keV) with a general-purpose low-energy collimator (*14*).

Conjugate views of opposed detectors are often used in quantitative measurements to compensate for attenuation (*16*). We, therefore, calculated the summed response for opposed detectors to show the reduction in variation in resolution with depth. These results are included in Table 2.

Phantom Measurements

Spherical hot sources were supported at various depths in a water-filled tank. The bottom surface of the cylindrical tank (20 cm in diameter and 20 cm high) was positioned 5 cm above the collimator with the camera pointing up. Therefore, in these experiments, source depths were measured from the bottom surface of the water tank. Two thin walled spherical sources [3.75 cm and 6.00 cm in inner diameter (i.d.)] were used to determine the dependence of attenuation on source size. The sources were uniformly filled with a known amount of ^{32}P (approximately 3.7 × 10^8 Bq of activity). Images (128 × 128 matrix) of the spheres at different depths were acquired with more than 200K counts per view. The reproducibility of the phantom measurements was within ±5% due to statistical errors, source positioning, and ROI selection.

Three circular ROIs were selected with varying diameters as follows. The first region (ROI1) fully enclosed the visual image boundary of the source. The radius of the second region (ROI2) was twice that of ROI1 (*14–15*). Finally, in order to compare ROIs between sources of different size, the distance between the edge of the source's visual image boundary and the edge of the selected ROI was kept consistent. Therefore, a third region (ROI3) for the large source was selected so that its radius equals the radius of ROI1 of the large source plus the radius of ROI1 of the small source.

TABLE 2
Resolution Parameters of the PSF for ^{32}P for Four Different Depths of the Sources in a 20-cm Deep Scattering Medium

Depth (mm)	FWHM (mm)	FWTM (mm)
Single Detector		
5	12.6	19.6
50	12.7	22.4
100	16.8	25.2
150	19.6	30.8
Conjugate Symmetry (50–150 mm range)		
50/150	16.2	26.6
100/100	16.8	25.2

Results are shown for single and opposed detectors. In the latter case, a 30-cm collimator separation was considered and the summed response for conjugate views was calculated.

Bremsstrahlung Energy Window

A broad energy window (57–285 keV) was empirically selected to enhance the sensitivity of detection and thus to compensate for the low geometrical efficiency of the collimator. The measured response (PSF) of the collimator for this broad energy window was found to be radially symmetric. Figure 1 shows the energy spectra recorded from a point source at four different depths in the water tank (*1*). The selected energy window was a combination of a 50% energy window centered at 76 keV and a 99% energy window centered at 190 keV. The former included the characteristic K-shell peak at approximately 82 keV to further enhance the detector sensitivity without apparent loss of spatial resolution as reported elsewhere (*2,7*). The measured sensitivity obtained for ^{32}P was 6 × 10^{-6} cps/Bq using equivalent NEMA specifications.

Resolution Recovery Filter

It has recently been demonstrated that the Wiener restoration filter partially compensates for the blurring effects of photon scattering and collimator penetration for single photon emitters of low and medium photon energy (*9,10*). We investigated the use of this filter for the high photon energies of ^{131}I (364 keV) and observed partial resolution restoration for the FWTM in particular, which reflects photon penetration effects through the collimator septa (*17*). The application of this filter to imaging bremsstrahlung was therefore considered.

The Wiener filter uses minimization of the mean square error between restored image and object function as the optimizing criterion. Wiener filtering exploits a priori estimates of the object and noise power spectra formed from the degraded image. The transfer function of the Wiener filter is (*8, 10*):

$$W(u, v) = \frac{1}{H(u, v)} \cdot \frac{|H(u, v)|^2}{\left[|H(u, v)|^2 + \frac{P_n(u, v)}{P_f(u, v)}\right]},$$

where $P_n(u, v)$ and $P_f(u, v)$ are the power spectra of the noise and signal processes respectively. $H(u, v)$ is the system transfer function at discrete frequency values u and v. If the PSF is stationary and assumed to be radially symmetric, then $H(u, v)$ can be replaced with the one dimensional system MTF, and the entire

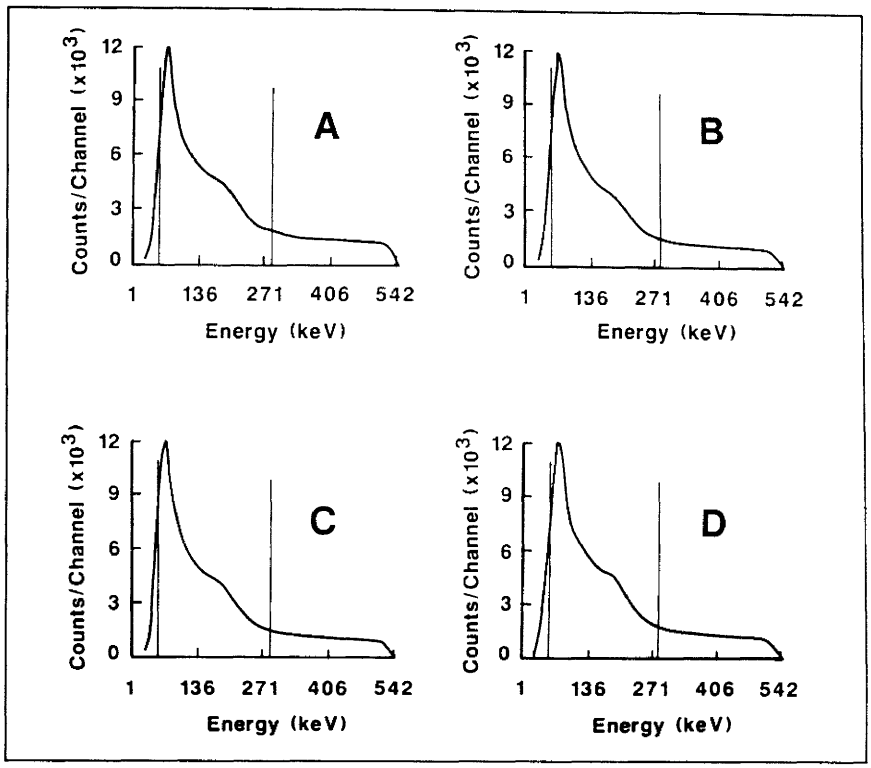

FIGURE 1. Bremsstrahlung energy spectra recorded from a point source of ^{32}P at (A) 5 mm, (B) 50 mm, (C) 100 mm, and (D) 150 mm depth in the scattering medium. The vertical lines indicate the selected energy window.

filter can be collapsed into one dimension (*10*):

$$W(f_r) = \frac{1}{MTF(f_r)} \cdot \frac{|MTF(f_r)|^2}{\left[|MTF(f_r)|^2 + \frac{P_n(f_r)}{P_f(f_r)}\right]},$$

where f_r is the radial frequency. Note that the filter can be considered as the product of an inverse filter with a low pass filter which accounts for the noise to signal ratio at each frequency. For images with a low noise-to-signal ratio, the filter reduces to the inverse filter. At frequency values for which the noise dominates, the noise-to-signal term becomes dominant and the filter assumes more of the low pass characteristic. In this sense, the filter adapts to the spectral properties of the image. In this work, the filter was optimized only for the idealized scattering medium and the discrete isolated spherical phantom sources. Furthermore, since the sources were imaged at various depths over a 20-cm range, a PSF taken at an average depth of 10 cm in the scattering medium was used in our calculations of the MTF.

RESULTS

Effective Attenuation Coefficient

Plots of the measured counts within ROIs selected for each depth of the source in the water tank are shown in Figures 2 and 3. The fraction of the detected counts within the image of the source decreased with increasing source

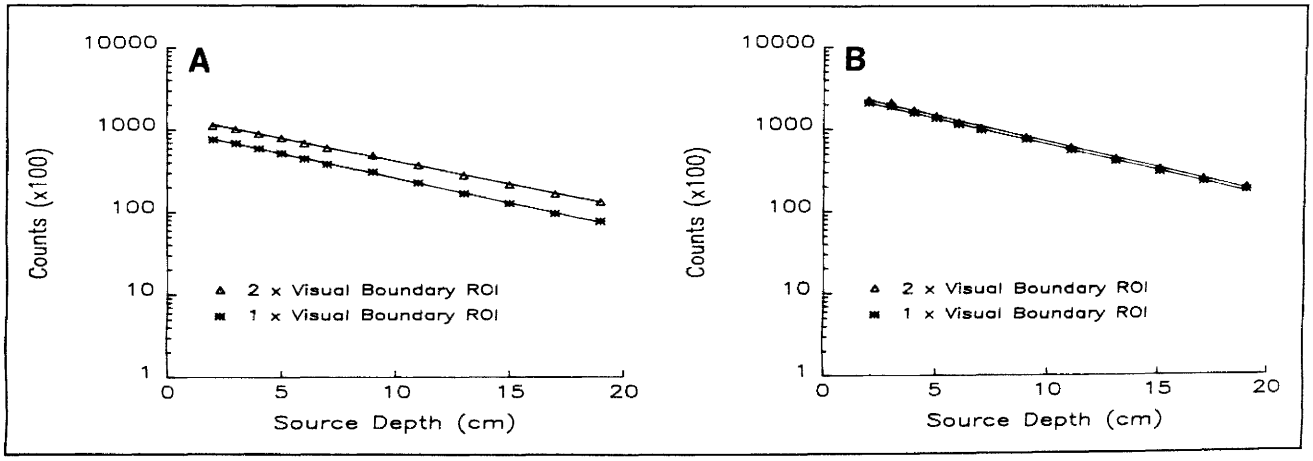

FIGURE 2. Linear regression fits to the experimental data from the small spherical source (i.d. = 3.75 cm). (A) Raw data and (B) Wiener filtered data versus source depth in scatter as a function of ROI size. "1 × Visual Boundary ROI" corresponds to ROI1 and "2 × Visual Boundary ROI" corresponds to ROI2.

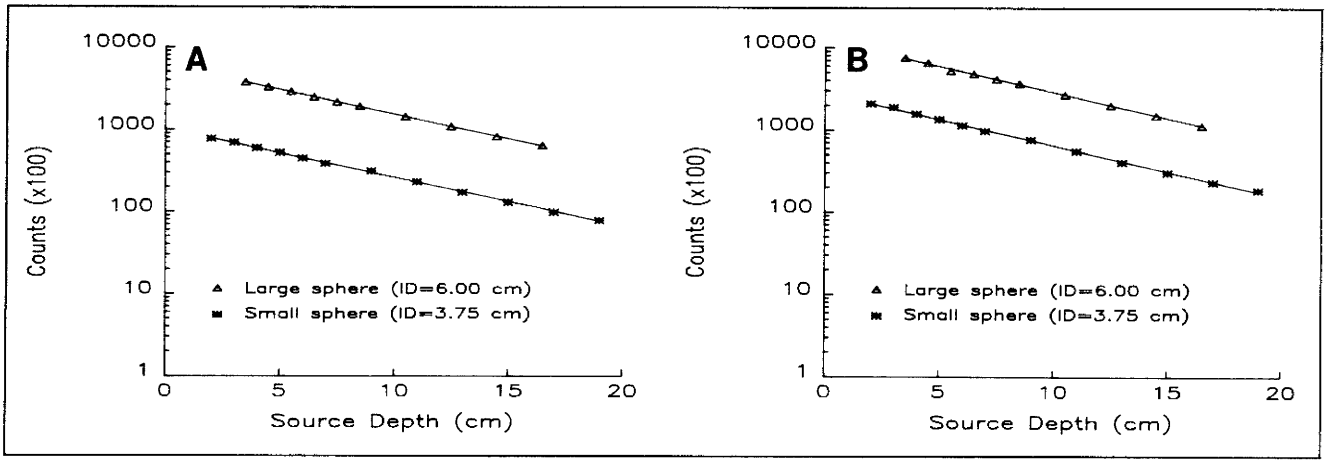

FIGURE 3. Linear regression fits to the experimental data from ROI1 of both sources. (A) Raw data and (B) Wiener filtered data versus source depth in scatter as a function of source size.

depth (*2*). Table 3 summarizes the values of the effective attenuation coefficient μ obtained from exponential regression fits to the experimental data. Also listed are the linear correlation coefficients which were greater than 0.99 despite the polychromatic photon flux. This result was partly attributed to the small variation in resolution of the long-bore collimator with depth (*1,2*). It may also be partly due to the broad energy window used and the small change in the shape of the bremsstrahlung spectrum as the depth of the source in the scattering medium increases (Fig. 1). These response characteristics were not observed with a conventional medium-energy collimator where the resolution and energy spectrum change with depth (*1,2*). The high degree of correlation in the measured data suggests that an effective linear attenuation coefficient can be applied for either planar gamma camera or tomographic measurements.

Influence of ROI, Source Size, and Filter

Figures 2 and 3 demonstrate that an effective linear attenuation coefficient can be measured irrespective of the size of the ROI, the size of the source, or the use of the resolution recovery filter. Table 4 lists the percent difference between the attenuation coefficients obtained from the ROIs described previously. The variations of the effective attenuation coefficient for bremsstrahlung with ROI and source size are comparable to those observed for single-photon emitters, particularly for medium to high photon energies which have a higher collimator penetration fraction (*15,16*). One should also note that the dependence of the effective attenuation coefficient on ROI or source size is similar for both raw and filtered data, i.e., within the experimental error of measurement.

Figure 4 shows a plot of the measured counts versus the size of the ROI area for the smaller sphere centrally located in the tank. Both raw and filtered data are presented. The fraction of the total counts observed within the visual boundary of the unfiltered image of the source was increased by a factor of approximately two when the image was filtered. The percentages of the total counts of an image within a selected ROI are listed in Table 5 for the two spherical sources. These results reflect the extent of the resolution recovery for bremsstrahlung for the idealized

TABLE 3
Calculated Values of the Effective Attenuation Coefficient μ and Corresponding Linear Correlation Coefficient of the Log of Counts Versus Source Depth for Each Given ROI

Source	ROI	Filtered	μ (cm^{-1})	Correlation
3.75 cm				
	ROI1	no	0.137	0.9996
		yes	0.146	0.9996
	ROI2	no	0.127	0.9997
		yes	0.136	0.9990
6.00 cm				
	ROI1	no	0.137	0.9998
		yes	0.143	0.9993
	ROI2	no	0.124	0.9999
		yes	0.134	0.9995
	ROI3	no	0.128	0.9993
		yes	0.139	0.9996

TABLE 4
Percent Difference Between the Values of the Effective Attenuation Coefficient Obtained from Different ROIs of the Same Source and Comparable ROIs of Different Sources

%Difference between ROI1 and ROI2			%Difference with source size		
Source	Raw data	Filtered	ROI	Raw data	Filtered
3.75 cm	8%	7%	ROI1 (both sources)	<1%	2%
6.00 cm	10%	7%	ROI2 (small source) & ROI3 (large source)	<1%	2%

The values listed in Table 3 were used for these calculations. Differences between raw data and filtered data were within experimental error of measurements (±5%).

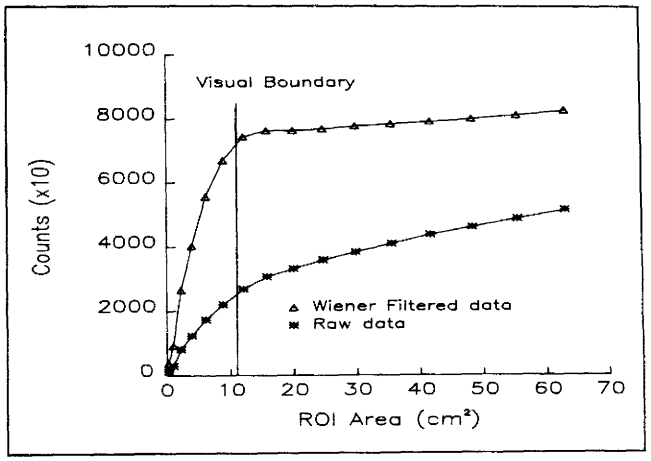

FIGURE 4. Plots of ROI counts versus ROI area for the small spherical source (i.d. = 3.75 cm) at a depth of 10 cm in the scattering medium. The visual boundary (ROI1) was, as indicated, essentially the same for the raw and filtered image. The fraction of total photons, however, detected within ROI1 is larger for the filtered image as shown in Table 5.

scattering medium and an isolated source. This is important when more than one source lies within the field of view of the gamma camera. In this case, it is necessary to minimize cross talk between adjacent sources in order to obtain an accurate value of the activity (*15*).

DISCUSSION

Imaging of bremsstrahlung has been reported by other investigators using the gamma camera and conventional low and medium energy collimators (*4–7*). The spatial resolution, based on obtained images, was estimated to be greater than 4 cm (FWHM). The detector's response to the imaged sources extended to their total field of view (FOV) because of the extent of photon penetration through the collimator septa. Broad energy windows were generally employed that were empirically determined. In some instances narrow energy windows were selected to enclose only the characteristic K-shell peak in an attempt to improve spatial resolution. In all instances, only approximate source localization was possible and no attempts were made to measure an effective attenuation coefficient for bremsstrahlung.

TABLE 5
Percentages of the Total Counts of an Image, Recorded at a Source Depth of 10 cm, Within a Selected ROI Before and After Filtering

Source	ROI	Raw data	Filtered
3.75 cm			
	ROI1	25.1%	62.4%
	ROI2	40.0%	66.4%
6.00 cm			
	ROI1	27.1%	51.7%
	ROI2	48.1%	61.2%

The fraction of detected photons within ROI1 is almost doubled after the application of the Wiener filter.

The work reported here is an experimental approach demonstrating the possibility of measuring an effective attenuation coefficient for bremsstrahlung using a highly collimated gamma camera and empirically selected energy windows. A high-energy collimator previously designed for therapy doses of medium to high photon energies such as ^{131}I was employed (*12*). Several medium-energy collimators were also previously evaluated (*2*). They exhibited, however, poor spatial resolution characteristics which varied significantly with depth. The PSF response for these collimators was also generally radially non-uniform.

The results reported here are from isolated sources within an idealized scattering medium with uniform attenuation and generation of bremsstrahlung. Under these constraints, an effective linear attenuation coefficient was measured. This coefficient was not strongly dependent on the size of the ROI or the size of the source. The use of the Wiener filter allowed the measurement of an effective attenuation coefficient which would be less dependent on the effects of cross talk between adjacent sources within the field of view of the detector, a situation frequently observed in antibody imaging. The above results should allow attenuation corrections to be performed using either the geometric mean of opposed detectors for planar imaging or Chang algorithm (*18*) for tomographic imaging with the gamma camera. We are currently investigating the possibility of performing quantitative imaging using the gamma camera with the long-bore collimator in the tomographic mode of detection.

The application of these methods to clinical investigations requires a more realistic model for localized variations of bremsstrahlung generation in tissue and for related photon transport mechanisms. Similarly, the resolution recovery observed with the Wiener filter was obtained for images of isolated or discrete (spherical) sources as opposed to more realistic measurements of clinical radionuclide distributions with different image and noise power spectra. Therefore, the amount of resolution recovery achieved will likely be overestimated for the case of extended sources where the signal power spectrum (P_f) decreases faster with frequency. The success of resolution recovery filters has recently been reported to be image dependent for single-photon emitters, particularly for images obtained in clinical investigations (*19*). The images obtained by bremsstrahlung detection, however, experience greater blurring due to enhanced photon scattering and penetration through the collimator septa. Hence, the application of the Wiener filter to bremsstrahlung may exhibit more resolution recovery than that observed for single photon detection. Our preliminary evaluation of filtered images ob-

tained during ^{32}P intraperitoneal therapy investigations showed promise of greater resolution recovery (*1*). Additional work and more realistic phantom models are required to optimize our methods for quantitative in vivo measurements of bremsstrahlung.

We are currently extending this work to include quantitative in vivo measurements of ^{90}Y-labeled antibodies as required for the management of radioimmunotherapy. The gamma camera should prove to have sufficient sensitivity for the larger radiation doses involved (4×10^8–18×10^8 Bq of ^{90}Y). The sensitivity for ^{90}Y should be approximately 1.5–2.0 times higher than the sensitivity reported here for ^{32}P because of its higher β-ray energy (2.27 MeV), which results in a higher conversion efficiency of the β-radiation to bremsstrahlung. The use of multidetector tomographic systems should further enhance the sensitivity for bremsstrahlung detection.

ACKNOWLEDGMENT

This work was supported by a grant from H. Lee Moffitt Cancer Center and Research Institute at the University of South Florida, Tampa, FL.

REFERENCES

1. Cullom SJ. Quantitative effects of Wiener restoration and attenuation correction on bremsstrahlung images with ECT. PhD thesis. University of South Florida; 1990.
2. Cullom SJ. Imaging of bremsstrahlung radiation from P-32 in nuclear medicine. Master's thesis, University of South Florida; 1987.
3. Clarke LP. Quantitative imaging methods for in-vivo management of antibody therapy. *Med Phys* 1989;16:512–513.
4. Balanchandran S, McGuire L, Flanigan S, Shah H, Boyd CM. Bremsstrahlung imaging after P-32 treatment for suprasellar cyst. *Int J Nucl Med and Biol* 1985;12:215–221.
5. Boye E, Lindegaard MW, Paus E. Whole-body distribution of radioactivity after intraperitoneal administration of P-32. *Br J Radiol* 1984;57:395–402.
6. Kaplan WD, Zimmerman RE, Bloomer WD, Knapp RC, Adelstein SJ. Therapeutic intraperitoneal P-32: a clinical assessment of the dynamics of distribution. *Radiology* 1981;138:683–688.
7. Ott RJ, Flower MA, Jones A, McReady VR. The measurement of radiation doses from P-32 chromic phosphate therapy of the peritoneum using SPECT. *Eur J Nucl Med* 1985;11:304–308.
8. King MA, Schwinger RB, Doherty PW, Penney BC. Two-dimensional filtering of SPECT images using the Metz and Wiener filters. *J Nucl Med* 1984;25:1234–1240.
9. King MA, Schwinger RB, Penney BC, Doherty PW, Bianco HA. Digital restoration of In-111 and I-123 SPECT images with optimized Metz filters. *J Nucl Med* 1986;27:1327–1336.
10. Penney BC, Glick SJ, King MA. Relative importance of the error sources in Wiener restoration of scintigrams. *IEEE Trans Med Imag* 1990;9:60–70.
11. Clarke LP, Cullom SJ, Kenny PJ, Saw CB, Silbiger ML. Quantitative ECT: comparison of recovery coefficient and linearity of detector response for single-photon and coincidence detection (F-18, β^+ 511 keV). *IEEE Trans Med Imag* 1986;MI-5:117–182.
12. Clarke LP, Saw CB, Leong LL, Serafini AN. SPECT imaging of I-131 (364 keV): importance of collimation. *Nucl Med Commun* 1985;6:41–47.
13. Cullom SJ, Clarke LP, Penney BC, King MA. SPECT: a novel method for bremsstrahlung imaging required for management of radioimmunotherapy (Y-90, P-32). [Abstract]. *Med Phys* 1989;16:469.
14. Harris CC, Greer KL, Jaszczak RJ, Floyd CE, Fearnow EC, Coleman RE. Tc-99m attenuation coefficients in water-filled phantoms determined with gamma cameras. *Med Phys* 1984;11:681–685.
15. Clarke LP, Qadir F, Al-Sheikh W, Sfakianakis GN, Serafini AN. Comparison of the physical characteristics of I-131 and I-123, with respect to differentiating the relative activity of the kidneys. *J Nucl Med* 1983;24:683–688.
16. Clarke LP, Malone JG, Casey M. Quantitative measurement of activity in small sources containing medium energy radionuclides. *Br J Radiol* 1982;55:125–133.
17. Cullom SJ, Clarke LP, Kenny PJ, King MA, Silbiger ML. Importance of collimation and restoration filter for quantitative imaging with I-131-labeled antibody (HMFG) [Abstract]. *J Nucl Med* 1989;30:876.
18. Chang LT. A method for attenuation correction in radionuclide computed tomography. *IEEE Trans Nucl Sci* 1978;NS-25:638–643.
19. King MA, Coleman M, Penney BC, Glick SJ. Activity quantitation in SPECT: a study of prereconstruction Metz filtering and use of the scatter degradation factor. *Med Phys* 1991;18:184–189.